Spatiotemporal dynamics of different growth-diffusion systems on a percolation lattice

Yiqin Liang,[1,*] Renlong Yang,[1,*] Yifan Guo,[2,*] Chongming Jiang,[3] Lizhi Liu,[4] Yanzi Wan,[1] and Yuanzhi Shao[1,†]

[1]*School of Physics, Sun Yat-sen University, Guangzhou 510275, China*

[2]*Department of Mechanical Engineering and Materials Science, Duke University, Durham, North Carolina 27708, USA*

[3]*Department of Microbiology and Immunology, Weill Cornell Medicine, Cornell University, New York, New York 10065, USA*

[4]*Sun Yat-sen University Cancer Center, State Key Laboratory of Oncology in South China, Collaborative Innovation Center for Cancer Medicine, and Guangdong Key Laboratory of Nasopharyngeal Carcinoma Diagnosis and Therapy, Guangzhou 510060, China*

(Received 25 June 2018; revised manuscript received 18 February 2019; published 2 April 2019)

To investigate the proliferation and invasion of a tumor within an inhomogeneous matrix, we studied the spatiotemporal dynamics of two types of growth-diffusion systems (GDSs) with logistic or Allee growth occurring on a two-dimensional square site percolation lattice via numerical computation and finite-size scaling approaches. A critical percolation threshold exists in the two systems, but becomes obscure with an increasing Allee effect in Allee growth. The two systems evidently differ in their short-time spatiotemporal patterns: The tumor number density in the logistic model grows and spreads continuously and subdiffusively or weakly superdiffusively while that in the Allee model does so discretely and strongly superdiffusively. This difference is attributed to a lack of cooperation between sites for growth and diffusion in the logistic model as compared to its Allee counterpart. The Allee growth pattern is characterized by a rougher border and more inhomogeneous interior than its logistic counterpart. Judging from their growth-diffusion feature in combination with a clinical image analysis, we conclude that Allee growth is more suitable for modeling the proliferation and invasion of an early-stage malignant tumor than is logistic growth. A phase diagram that correlates a tumor's growth and diffusion on a percolation lattice with a site occupation fraction and Allee effect was established to reveal the sensitivity on proliferation and spreading of a tumor towards the above parameters. The Allee effect was also found to induce diverse dynamic features on its short-time growth and diffusion in the GDS, which brings in an opposite trend toward a tumor's growth and diffusion.

DOI: 10.1103/PhysRevE.99.042401

I. INTRODUCTION

A logistic model is a typical dynamical system that is usually applied to evaluate the growth of a biological system [1,2], e.g., the growth of tumor cells [3–5]. However, ever-increasing evidence has shown that the growth and diffusion of a tumor are possibly regulated by the Allee effect [6,7], e.g., cooperation among cells might be required to produce proangiogenic growth factors for tumor proliferation such as the vascular endothelial growth factor (VEGF), which recruits blood vessels to irrigate the tumor [8]. The Allee growth model addresses the importance of a minimum number density of tumor cells not considered by the logistic model for restricting the proliferation and growth of a tumor. In 2016, Allee growth was employed to model the growth of a malignant tumor without considering the inhomogeneity of the microenvironment [9]. The logistic model simply involves a competition between individual species to restrict individual growth due to a limited carrying capacity, while the Allee model includes intraspecific cooperation as well as competition suggested by the logistic model [10]. In the Allee model, if members of an individual cannot cooperate efficiently [11], the species will decrease in its density, and even die out, although resources with low intraspecific competition are abundant in the environment. Evaluating how such an intraspecific cooperation against competition impacts the spatiotemporal behavior of a biological system in an inhomogeneous system, e.g., percolating lattices, is an intriguing topic.

Anomalous diffusion in an inhomogeneous system occurs ubiquitously in a variety of disciplines such as physics, chemistry, and material science [12,13]. Inhomogeneity in the structure of a system has a profound effect on the transport characteristics of the system, e.g., the critical conductivity at the percolation threshold on a geometrical percolating lattice cluster [14]. Anomalous diffusion fails to observe the Fickian law of diffusion [15]. Different from what happens to pure diffusion in a simple diffusion system, either proliferative or extinctive behavior appears in growth-diffusion systems (GDSs) together with diffusion. Transportation of reaction-diffusion (RD) systems on a two-dimensional (2D) percolating lattice cluster has been studied by a few researchers [16], including the system affected by the Allee effect [17]. David *et al.* recently reported the application of a logistic RD system to investigate the effect of stress on glioma growth and diffusion in a conventional three-dimensional (3D) space [18], which focuses on a specific GDS. Generally, the GDS can be classified into the same category as the RD system. Nevertheless, the GDS possesses some diverse dynamical biological features, such as the multistate coexistence of an opposite trend toward growth versus diffusion that we address in the

*These authors contributed equally to this work.

†stssyz@mail.sysu.edu.cn

 ©2019 American Physical Society

current paper. Specifically, the logistic model and Allee model are of a linear and nonlinear growth in nature, respectively, according to their characteristics of per capita proliferation [17]. An intriguing question is raised as to whether a critical threshold of the percolation lattice exists for the above two different GDSs. What law will it obey, if it exists, as well as what is the implication for a tumor's proliferating and infiltrating within an inhomogeneous matrix that it will impart from the corresponding spatiotemporal patterns? The current paper intends to address the two questions.

The paper consists of four sections: an introduction, methods and models, results, and a summary with conclusions. The second section describes the GDS, percolating lattice, and the algorithms; the third section demonstrates the simulation results, a finite-size scaling (FSS) analysis, a fractal analysis of images, and an anomalous diffusion analysis; and the fourth section summarizes this study and draws the conclusions of this paper.

II. METHODS: MODELING AND ANALYZING

A. Logistic model and Allee model

Equations (1) and (2) are the dynamic equations of the logistic model and the Allee model, respectively,

$$\frac{dn(t)}{dt} = r\,n(t)\left[1 - \frac{n(t)}{K}\right], \tag{1}$$

$$\frac{dn(t)}{dt} = r\,n(t)\left(1 - \frac{n(t)}{K}\right)\left(\frac{n(t)}{A} - 1\right), \tag{2}$$

where n, t, r, K, and A denote the species number density, evolution time, proliferation rate, environment carrying capacity ($n < K$), and the intensity of the Allee effect, respectively.

The number density of the logistic model evolves to an equilibrium state regardless of its initial value, while the final evolution result of the Allee model, depending on its initial value, can be divided into three states (equilibrium, approaching K, and extinction) [see Fig. S1 of the Supplemental Material (SM) [19]]. The carrying capacity characterizes the intraspecific competition between species members [20], while the intensity of the Allee effect reflects the intraspecific *adaptive cooperation* of the members [11]. The Allee effect can be generally classified into two categories, namely, a strong Allee effect ($A > 0$) and a weak Allee effect ($A < 0$) [21]. The current study is confined to the strong Allee effect, and the intensity of the strong Allee effect is further categorized for convenience of analysis. In the case of $A < n$, the smaller A is, the weaker is the Allee effect, which leads to a better intraspecific adaptive cooperation with a rapid increase in the number density n; in the case of $A > n$, however, the intraspecific adaptive cooperation is negative, and the number density undoubtedly declines throughout the evolution with a negative growth; in the case of $A = n$, the number density evolves with a zero growth [22]. A noticeable fluctuation of the number density is observable when n fluctuates slightly around A nearby. That is because the sign of dn/dt changes alternatively, therefore the growth of the species with the Allee effect fluctuates remarkably. We refer to the fluctuation above as the *intrinsic fluctuation* of Allee growth, which is inevitable for Allee spatiotemporal growth.

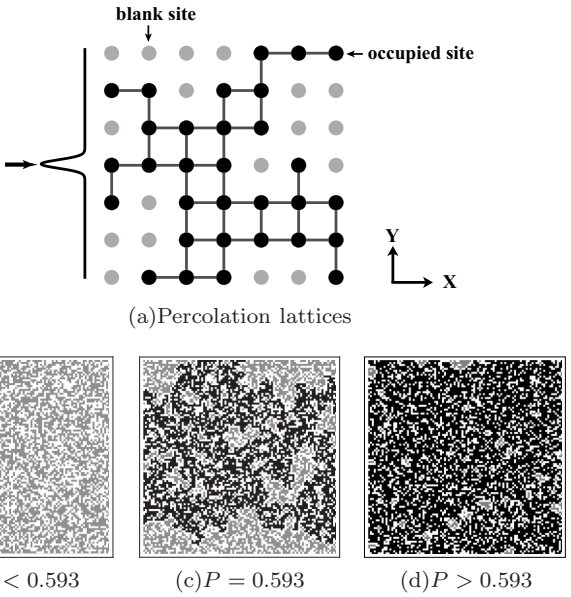

FIG. 1. (a) The schema of a site percolation lattice; (b)–(d) the connectivity of the clusters with different site occupation probabilities.

B. Percolation lattice of the growth environment

Simple 2D square site percolation lattices were employed in this study. Figure 1(a) shows the configuration of a square percolation lattice with a size of $L \times L$. When a site percolation lattice is constructed, every site is either randomly occupied or blank according to the site occupation probability P. The occupied sites are supposed to be randomly distributed on the lattice with a proportion that is equal to P, and the blank sites with a proportion $1 - P$.

The Cartesian coordinate (x, y) was adopted to locate every site, and it was rescaled by L,

$$x' = \frac{x}{L}, \quad y' = \frac{y}{L}. \tag{3}$$

According to the percolation theory, the percolation threshold of a 2D square site lattice P_c is 0.592 746 [23]. Figures 1(b)–1(d) show the connectivity of the clusters when P is less than, equal to, or greater than P_c, respectively (at $L = 50$). When $P \geqslant P_c$, a global cluster is formed that spans from one edge of the lattice to the other. The cluster is permeable for many physics properties such as electricity, heat, and mass transportation in a pure diffusion environment. For the GDS addressed in this paper, we defined a site occupation fraction Q, similar to the site occupation probability P of a common percolation without growth, to quantify the growth and spread among the occupied sites. A larger site occupation fraction Q is equivalent to a more homogeneous state of a percolation lattice. The evolution of the number density is presumed dependent on the site occupation fraction Q instead of P in a conservative system because the number density n is not conservative in the GDS. In the case of extinctive species, even if a globally connective cluster emerges, the species still fails to span the percolation lattice because of its unsurvivable number density. In the GDS, the situation that a survivable number density can span the globally connective cluster is defined as the successful penetration (SP) of species.

A minimal Q to realize the SP is referred to as the SP threshold or the critical point, denoted as Q_c. Therefore, it is reasonable to assume $Q_c \geqslant P_c$. Owing to the randomness of the configuration of percolation lattice, simulations with the same parameters were performed repeatedly (unless specified, the default repeat was set to 10 000 times, and L was set to 50). The ratio of the repeat number of SP occurrence against the total simulation is defined as the probability of penetration R, which is used in this paper to account for the invasion of an *in silico* tumor inside an inhomogeneous matrix. Note that although the growth and diffusion is isotropic, the way to record the SP and the definition of R are characteristics of directed percolation. All computations were performed on the Tianhe-2 supercomputer at the National Supercomputing Center (NGCC) in Guangzhou, China.

C. The growth-diffusion model of a tumor

The spatiotemporal patterns of both logistic (Fisher-Kolmogorov [24]) and Allee growth and diffusion on a site percolation lattice are used to describe the growth and invasion of a tumor inside an extracellular matrix in this paper. In light of the tumor biology, the inhomogeneity of a tumor's growth environment imposes a huge impact on the growth and invasion of tumors [25,26]. The percolation lattice is introduced in this paper to imitate such an inhomogeneity of the tissue surrounding a tumor with the growth-diffusion process regulated by the Allee effect.

The dynamic equation of number density n with growth and diffusion is expressed as

$$\frac{dn}{dt} + \nabla \cdot \boldsymbol{J} = S_n, \tag{4}$$

where $\boldsymbol{J}$ denotes the number density current, and S_n denotes the net proliferation of cells.

Proliferation and diffusion are the main concerns of this paper. The number density current $\boldsymbol{J}$ is supposed to obey the following relationship,

$$\boldsymbol{J} = -D\,\nabla n, \tag{5}$$

where D is a diffusion coefficient.

S_n is related to proliferation and extinction, which can be set as, e.g., the Allee growth function,

$$S_n = r\,n\left(1 - \frac{n}{K}\right)\left(\frac{n}{A} - 1\right). \tag{6}$$

For computational convenience, the quantities in Eqs. (3)–(6) were rescaled as follows,

$$\widetilde{n} = \frac{n}{n_{\text{ref}}}, \quad \widetilde{x} = \frac{x'}{l_{\text{ref}}}, \quad \widetilde{y} = \frac{y'}{l_{\text{ref}}}, \quad \widetilde{\tau} = \frac{t}{\tau_{\text{ref}}},$$
$$\widetilde{d} = \frac{\tau D}{l_{\text{ref}}^2}, \quad \widetilde{r} = r, \quad \widetilde{K} = \frac{K}{n_{\text{ref}}}, \tag{7}$$

where l_{ref} represents the maximum invasion distance of the tumor; τ_{ref} denotes the time of the cell division cycle; and n_{ref} is the reference value of the tumor number density.

Dropping the tildes above the variables, we can obtain the dimensionless partial differential equation (PDE),

$$\frac{\partial n(t)}{\partial t} = \nabla \cdot (D\,\nabla n) + r\,n(t)\left(1 - \frac{n(t)}{K}\right)\left(\frac{n(t)}{A} - 1\right). \tag{8}$$

TABLE I. Meanings and values of the parameters in the simulation models.

Symbol	Description	Dimensional value
l_{ref}	Length	1 cm [27]
τ_{ref}	Time	8–24 h (16 h) [27]
n_{ref}	Reference tumor cell density	6.7×10^7 cells cm^{-3} [28]
D	Diffusion coefficient	1×10^{-11} cm^2/s [29]
r_0	Tumor growth rate	$1.0/\tau$ [5]
K	Environment carrying capacity	$10 n_{\text{ref}}$ [5]
ϵ	Positive parameter	0.00025 [30]

D. Parameters for simulation

Randomly sweeping the percolation lattice was implemented before each simulation. A free boundary condition was used and the initial number density is supposed to be distributed along the left vertical boundary. The initial distribution was set to be a narrow Gaussian distribution along the left boundary, as shown in Fig. 1(a), and its mathematical form is expressed as

$$\widetilde{n}(\widetilde{x}, \widetilde{y}, \widetilde{\tau})|_{\widetilde{\tau}=0} = \begin{cases} \exp\left(-\frac{(\widetilde{y}-0.5)^2}{\epsilon}\right), & \widetilde{x} = 0, \\ 0, & 0 < \widetilde{x} \leqslant 1, \end{cases} \tag{9}$$

where $0 \leqslant \widetilde{y} \leqslant 1$. Other parameters are listed in Table I.

E. Finite-size scaling transformation

Through the finite-size scaling (FSS) approach of simulated percolation clusters, we can determine the percolation transition point Q_c and the corresponding critical exponents. Take the magnetic susceptibility χ in a ferromagnetic system as an instance, and the FSS formula for this system is [31]

$$\chi(\epsilon, L) = L^{\gamma/\nu} F(L/\xi) = L^{\gamma/\nu} f(\epsilon\, L^{1/\nu}), \tag{10}$$

where L is the characteristic length of a finite system; ν is the critical exponent of the correlation length; γ is the critical exponent of magnetic susceptibility; ξ is the correlation length of an infinite system at reduced temperature ϵ; and F and f are the corresponding scaling functions.

The probability of the SP event is denoted as $R(q, L)$, and an ansatz was adopted that conforms to the FSS transformation analogous to Eq. (10). Thus, the FSS criterion for the SP probability was rewritten as

$$R(q, L) = L^{\gamma/\nu} F(L/\xi) = L^{\gamma/\nu} f(q\, L^{1/\nu}), \tag{11}$$

where γ denotes the critical exponent of the SP probability, and the parameter definitions are kept the same as in Eq. (10).

Define q as

$$q = \frac{Q - Q_c}{Q_c}. \tag{12}$$

This parameter signifies the scaled difference between Q and Q_c and is referred to as the relative occupation fraction in this paper. As Q approaches Q_c, q is equal to 0. According to Eq. (11), the curves of the scaling functions for different lattice sizes L cross at the critical point where q is equal to zero. The general FSS function can be obtained by transforming the data of systems of different lattice sizes.

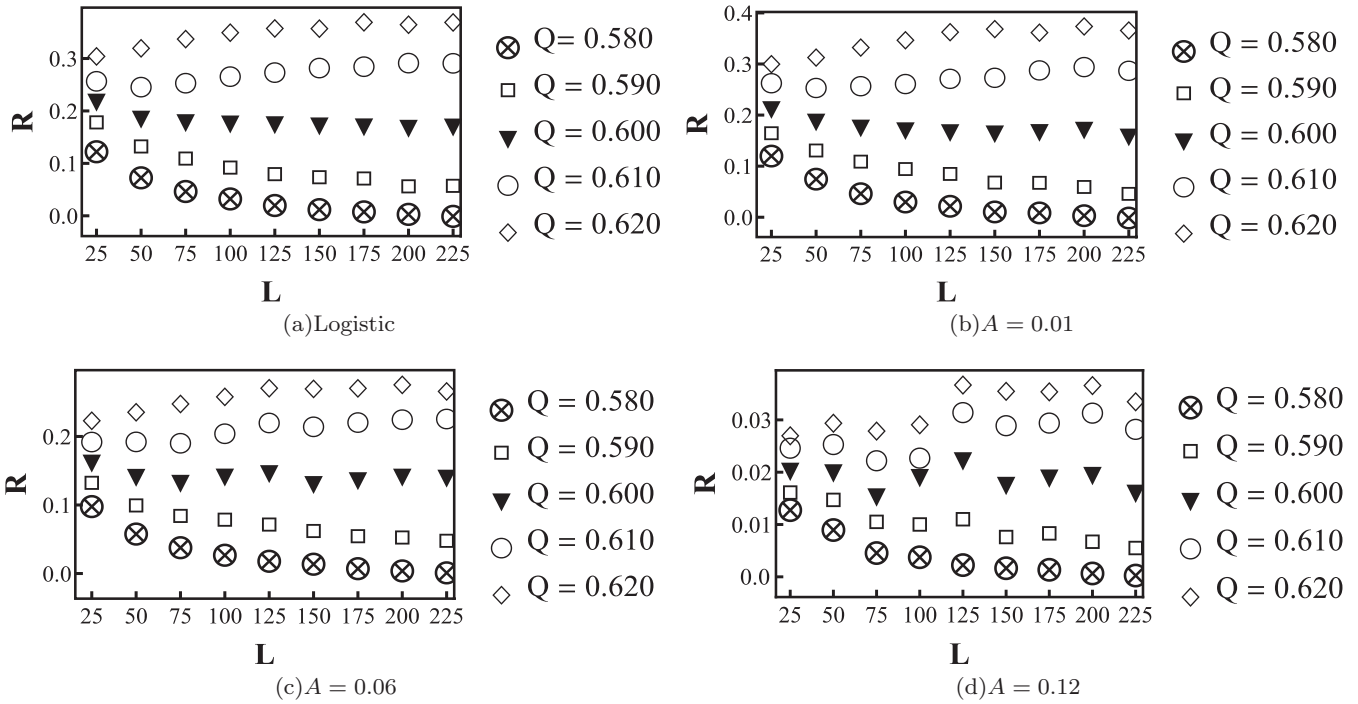

FIG. 2. The relationship between the probability of number density penetration R and percolation lattice size L at different site occupation fractions Q. (a) Logistic model and (b) Allee model with different intensities of the Allee effect, $A = 0.01$, (c) $A = 0.06$, and (d) $A = 0.12$. The lattice size L ranges from 25 to 225 with a step of 25. Q is the site occupation fraction, selected from 0.58 to 0.62 with a step of 0.01. Every data point in the figure is the average value after 10 000 simulations.

Spearman's rank correlation coefficient algorithm [32,33] was used to appraise the degree of overlap consistency for different curves, and only those results with the best consistency were acceptable for the scaled data. The SP threshold Q_c, and its critical exponents (γ/ν and $1/\nu$), were calculated using the transformed FSS function $R(q, L)$.

III. RESULTS AND ANALYSIS

A. Probability of penetration of tumor number density

The penetration probability of the tumor number density in the GDS depends on the initial number density, the configuration of a square percolation lattice, and specific growth models, which differ from the pure diffusion occurring in a conventional percolation lattice. Figure 2 displays the dependence of the SP probability R upon lattice size L with different site occupation fractions Q in the logistic model and Allee model at three different intensities ($A = 0.01$, $A = 0.06$, and $A = 0.12$). As judged from Fig. 2, the critical point exists at $Q = 0.600$ because R presents an inverse trend around $Q_c = 0.600$, indicating that the number density maintains a constant probability of penetration $R_c = 0.2$ at the critical point $Q_c = 0.600$ in the logistic model. The growth with a small Allee effect takes on a similar trend as that of the logistic model. However, when the Allee effect gets strong enough, R begins to fluctuate around the critical point and the exact value of Q_c becomes obscured. Moreover, the probability of penetration sharply decreases to 0.02 in this situation, inferring that the Allee effect can destroy the penetration of the tumor number density in the percolation lattice. When the Allee effect A exceeds 0.12, R will approximate to zero, and the critical point Q_c will disappear eventually.

Figure 3 is plotted from those original data of Fig. 2 through the FSS transformation according to Eq. (11). After this transformation, all probabilities of the penetration of the tumor number density in both logistic and weak Allee growth can be fitted with a universal scaling curve regardless of the lattice size. However, when the Allee effect is too strong ($A = 0.12$), the data points diverge apparently at the critical point ($q = 0$). There is no smooth scaling curve available within the data range, indicating that the characteristic of the percolation threshold is no longer distinct. The percolation threshold and other critical parameters were calculated using Spearman's rank correlation method, as listed in Table II. In addition, another approximate method was employed to estimate Q_c of an infinite percolation lattice (0.601 for the logistic and 0.595 for the Allee model, respectively) via approaching asymptotically $1/L \to 0$ (see Sec. S2, Figs. S2 and S3 of the SM [19]). The FSS analysis makes clear that the critical

TABLE II. Percolation threshold Q_c, critical exponent γ/ν and $1/\nu$, and Spearman's rank correlation coefficient ρ of the logistic and Allee model.

	Reference value	Logistic	$A = 0.01$	$A = 0.06$	$A = 0.12$
Q_c	0.5927 [23] (P_{cl})	0.592	0.592	0.594	~0.600
γ/ν	$5/48 = 0.1042$ [23]	0.39	0.39	0.26	~0.19
$1/\nu$	0.75 [34]	0.82	0.82	0.81	~1.00
ρ	N/A	0.9991	0.9987	0.9986	0.9947

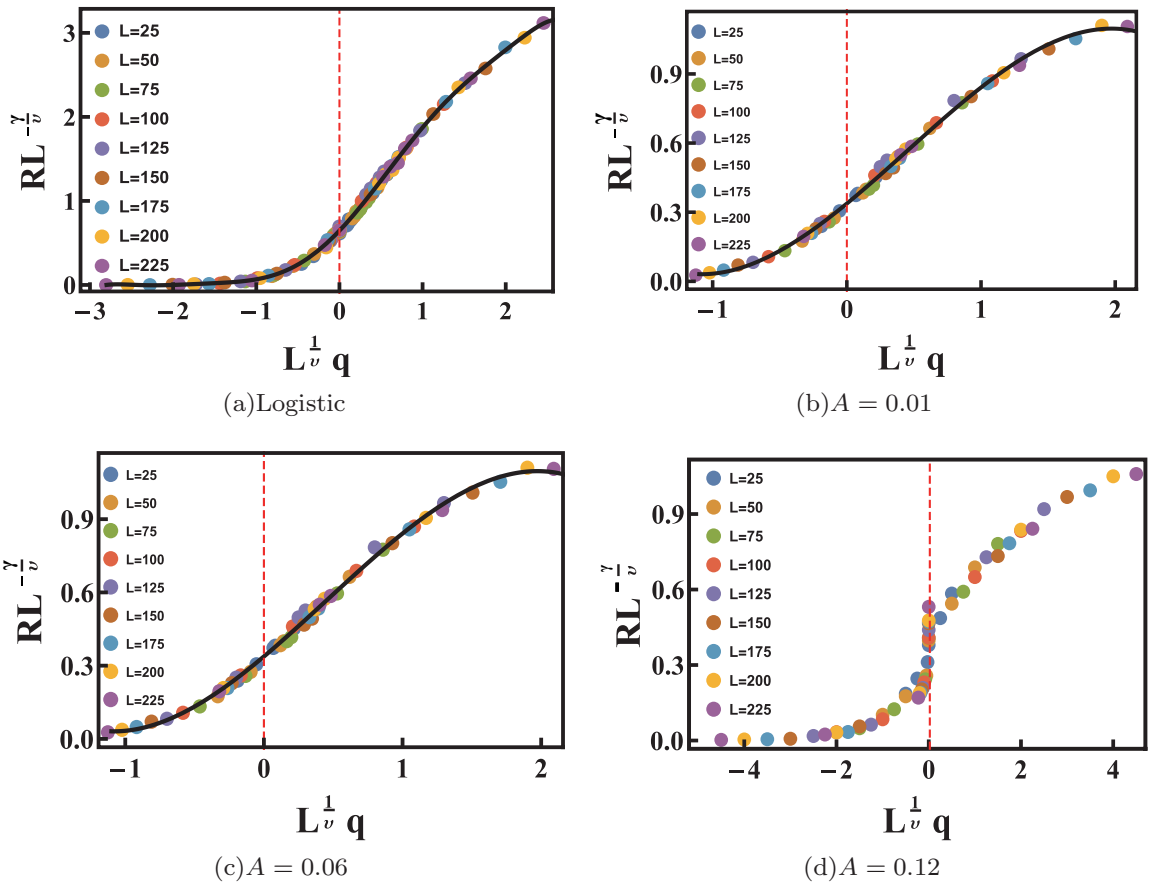

FIG. 3. Results of the FSS transformation with various percolation lattice sizes. (a) Logistic model, (b) Allee model with $A = 0.01$, (c) Allee model with $A = 0.06$, and (d) Allee model with $A = 0.12$. Red dashed lines show the critical points ($q = 0$) for each case. All resulting data were processed through the FSS transformation from the original data of Fig. 2.

value Q_c almost remains unchanged but the critical exponent varies remarkably when the growth and diffusion of a tumor are taken into account in the GDS, as compared to the pure percolation threshold P_c in a regular 2D square lattice without growth. This finding reveals that growth and diffusion on a percolation lattice not only keep the characteristics of simple percolation, but also bring in, due to the different growth term involved, different features in the probability of penetration. Furthermore, the values of Q_c and $1/\nu$ are almost invariant constants while γ/ν decreases with increasing Allee effect A. According to the theory of phase transition, the probability of penetration R obeys the relationship $R \sim q^{-\gamma}$. Therefore, a decrease in the critical exponent γ gives rise to a rapid decline of the probability of penetration, leading to an extremely significant fluctuation and sensitivity of R at the critical point.

B. Spatiotemporal growth features of the logistic and Allee model

Figure 4 displays the spatiotemporal patterns of the logistic and Allee model ($A = 0.02$) in a homogeneous ($Q = 1$) and inhomogeneous lattice ($Q = 0.9$), respectively. Note that the number density of the Allee model, even on the homogeneous lattice ($Q = 1$), grows discretely, which is in sharp contrast to the homogeneous and continuous growth of the logistic model. The difference above should be attributed to the peculiar adaptive cooperation between neighboring sites for growth and diffusion involved in the Allee model. Due to the interplay of the intrinsic fluctuation and the adaptive cooperation in the Allee model, the number density of Allee growth varies from site to site, featured with a fluctuating spatiotemporal pattern.

The proliferation of tumor cells in this paper is evaluated by the site-averaged number density of the tumor (denoted by $\bar{n}_{xy}$), which is defined as

$$\bar{n}_{xy} = \left(\sum_{x=1}^{L}\sum_{y=1}^{L} n_{xy}\right) \Big/ L^2. \tag{13}$$

The evolution curve of the spatiotemporal patterns in Fig. 4 was calculated with Eq. (13), and Fig. 5 displays two typical curves of them. The evolution curves are present in the site-averaged growth of the two models and also embody the difference between the growth pattern of those models. In the logistic model, the number density grows slowly and smoothly; growth in the Allee model, however, is much faster due to the adaptive cooperation between neighboring sites.

Note that the adaptive cooperation that varies from site to site exists, which gives rise to $\bar{n}_{xy}$ fluctuating and eventually reaching a state of dynamic equilibrium even in a homogeneous lattice ($Q = 1$). The inhomogeneous

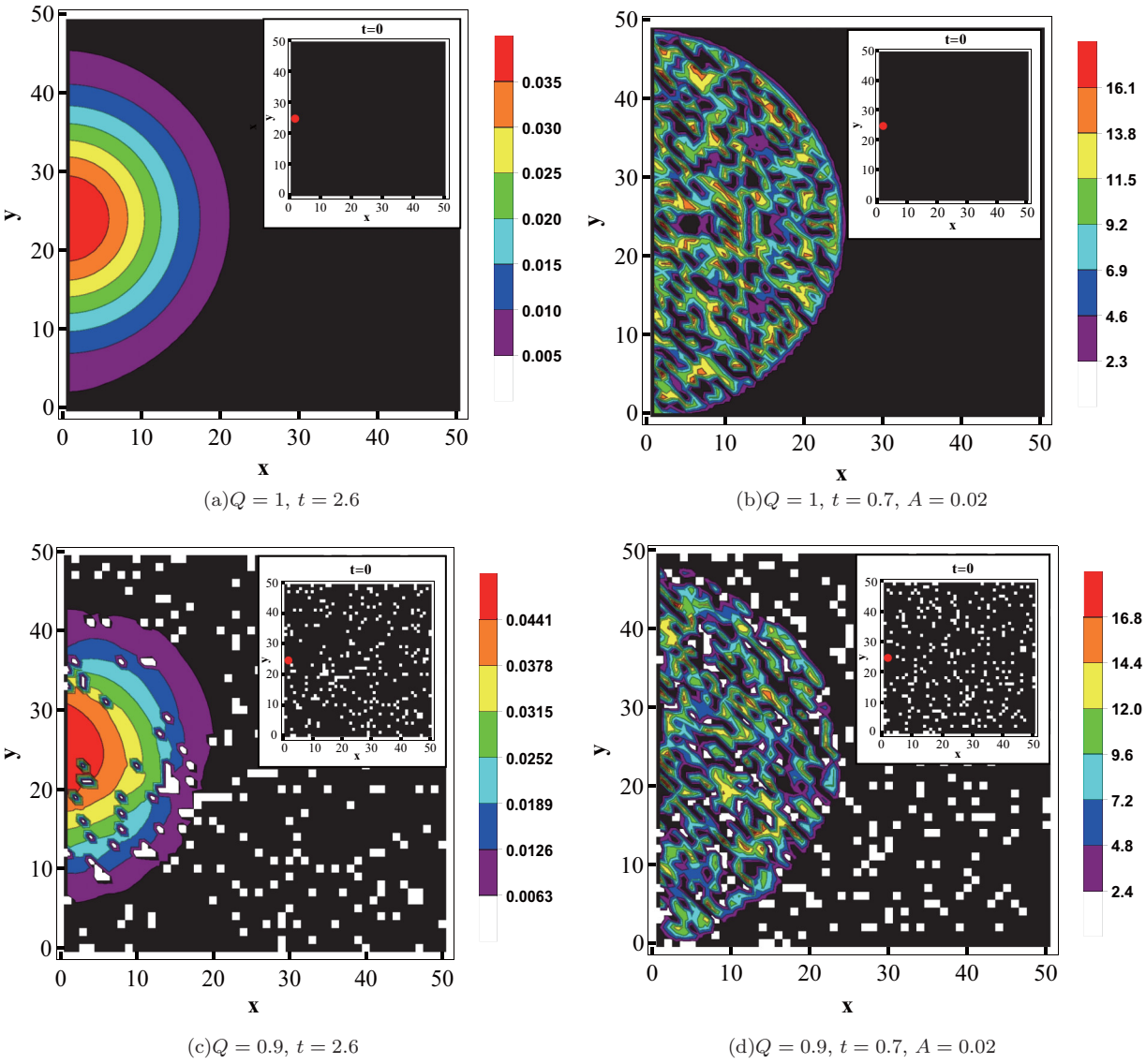

(a)$Q = 1,\ t = 2.6$ (b)$Q = 1,\ t = 0.7,\ A = 0.02$

(c)$Q = 0.9,\ t = 2.6$ (d)$Q = 0.9,\ t = 0.7,\ A = 0.02$

FIG. 4. Snapshots of the growth-diffusion patterns with the lattice size L set to 50×50. (a) and (b) are growth-diffusion patterns of the logistic model and Allee model on a percolation lattice with $Q = 1$ (homogeneity). (c) and (d) are growth-diffusion patterns of the logistic model and Allee model on a percolation lattice with $Q = 0.9$ (inhomogeneity). The inset is the initial distribution of the corresponding figure where the red point represents the initial position of a tumor.

($Q \neq 1$) counterpart has a similar trend (see Fig. S4 of the SM [19]).

For a more comprehensive study of the growth-diffusion patterns of the two models, the border fractal dimensions and a multifractal spectral analysis of the spatiotemporal patterns were applied to quantify the roughness of a tumor's border and its inner inhomogeneity.

The regular sandbox algorithm was employed to calculate the multifractal spectrum [35], and border fractal dimension data were extracted by the commercial software Image Pro Plus (IPP). Figure 6 exhibits the multifractal spectra of the logistic and Allee growth patterns in Fig. 4. Viewed from Fig. 6, broader multifractal spectra $\Delta\alpha$ of the Allee model are observed than that of the logistic model, implying that the Allee growth pattern possesses a larger spatiotemporal inhomogeneity. Moreover, the measured border fractal dimension of the Allee growth pattern is larger than that of the logistic one, meaning that the border of the Allee growth spatiotemporal pattern is characterized by greater roughness and openness. Details of these can be found in the SM (see Figs. S5 and S6 [19]). In general, the growth patterns of the two models differ remarkably in their border fractal dimension and inner multifractal spectra.

C. Comparison of spatiotemporal growth patterns of the logistic and Allee model with clinical tumor growth

In light of tumor biology and clinical medicine, the border of a malignant tumor is characterized by its openness and infiltration due to a plentiful nutrient blood supply in the extracellular matrix surrounding a malignant tumor, manifesting a rougher border with a larger fractal dimension [36]. Clinical images of 43 malignant breast tumors and 21 benign breast tumors were selected by our radiologist to measure

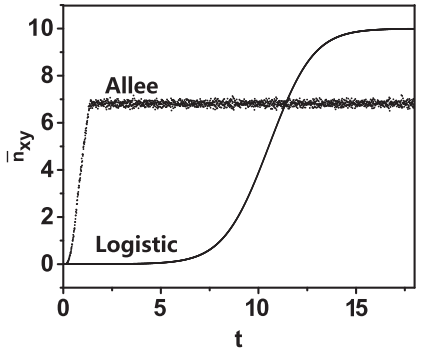

FIG. 5. The evolution of site-averaged number density of the logistic model and the Allee model on homogeneous lattices with the lattice size set to 50 × 50.

their fractal dimensions. The resulting fractal dimensions and those of logistic and Allee growth are shown in Fig. 7 for a comparison. Figure 7(a) indicates that the measured fractal dimension of a malignant breast tumor (M) is larger than that of its benign counterpart (B); the fractal dimensions of the Allee model are greater than those of the logistic model. In light of its larger border fractals and broader multifractal spectra, as well as fast growing and spreading pattern, the Allee model is confirmed to be more suitable for describing the early-stage growth of a malignant tumor than its logistic counterpart in the GDS. The figure also exhibits the influence of the Allee effect A on fractal dimension. Figure 7(b) shows that at the same Q, the weaker the Allee effect is, the larger is the border fractal dimension of the growing pattern. The results above indicate that a weaker Allee effect can give rise to larger border fractals of spatiotemporal patterns in the GDS.

D. Spatiotemporal diffusion features of logistic and Allee growth

To discriminate the diffusion feature of logistic and Allee growth that occurs on percolation lattices, the root-mean-square displacement of the number density r_n (see Sec. S9 of the SM [19]) versus the evolution time t was fitted numerically using the least-squares method with a power function,

$$r_n = at^b, \tag{14}$$

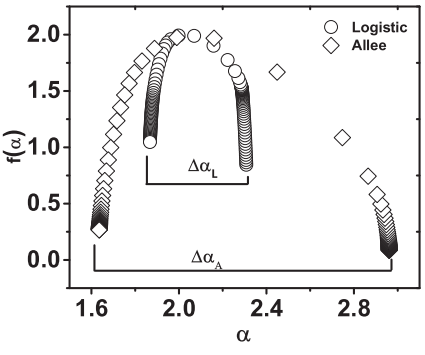

FIG. 6. Inner multifractal spectra of the growth patterns of the logistic and Allee model on a homogeneous lattice ($Q = 1$). α denotes the singular index of the number density and $f(\alpha)$ represents the fractal spectra.

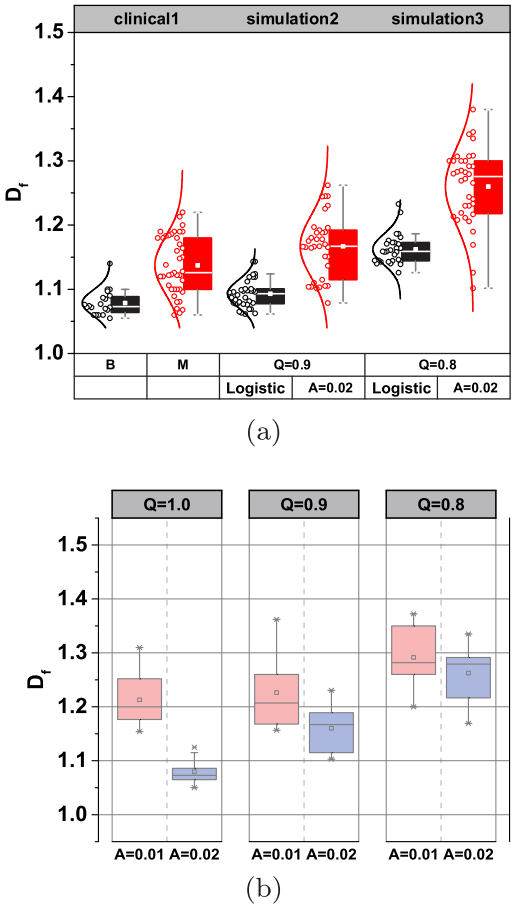

FIG. 7. (a) Box plot of border fractal dimensions for the clinical MRI images of benign and malignant tumors as well as the simulation models (logistic and Allee model) with $Q = 0.8$ and 0.9. (b) Box plot of border fractal dimensions of the simulation model (Allee model) under different Allee effects with $Q = 1.0$, 0.9, and 0.8, respectively, with each box plot containing 15 data points. The lattice size is set to $L = 50 \times 50$ in (a) and (b).

where a and b denote the diffusion constant and the exponent, respectively. The situations of $b < 0.5$, $b = 1/2$, $b > 0.5$, and $b = 1.0$ describe subdiffusion, Fickian diffusion, superdiffusion, and ballistic diffusion, respectively [37].

Figure 8(a) displays the short-time evolution of the root-mean-square displacement with respect to different Q in the logistic model; Fig. 8(b) shows the corresponding diffusion exponent. The data points of b distribute around 0.5, meaning that diffusion of the number density is enhanced from subdiffusion to superdiffusion as a percolation lattice becomes more homogeneous. The Allee model counterparts are shown in Figs. 8(c) and 8(d). The two figures illustrate that more significant diffusion of the short-time evolution dynamic occurs in the Allee model with a larger b than its logistic counterpart. Increasing spatial homogeneity further brings about diffusion, transforming from superdiffusion to ballistic diffusion in the Allee model.

This study also made a preliminary simulation of the long-term dynamic behavior of the two growth systems on an extended percolation lattice $L = 500 \times 500$. On a homogeneous lattice ($Q = 1$), the time evolution of root-mean-square

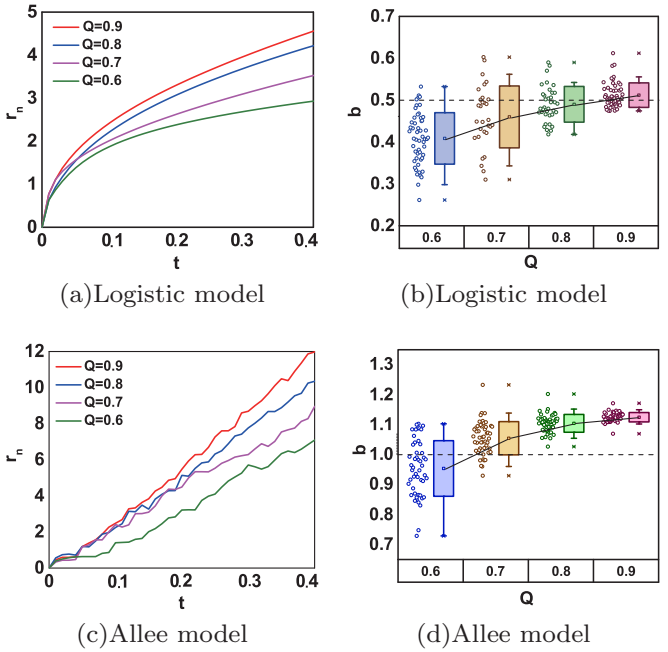

FIG. 8. (a) and (c) show the typical time evolution of root-mean-square displacement of the number density in the logistic model and Allee model ($A = 0.02$) with different percolation lattices ($Q = 0.9$, 0.8, 0.7, and 0.6). (b) and (d) present the box plots of 50 sets of data points of diffusion exponents b in the logistic model and Allee model ($A = 0.02$) with different percolation lattices ($Q = 0.9$, 0.8, 0.7, and 0.6). The lattice size is set to $L = 50 \times 50$ from (a) to (d).

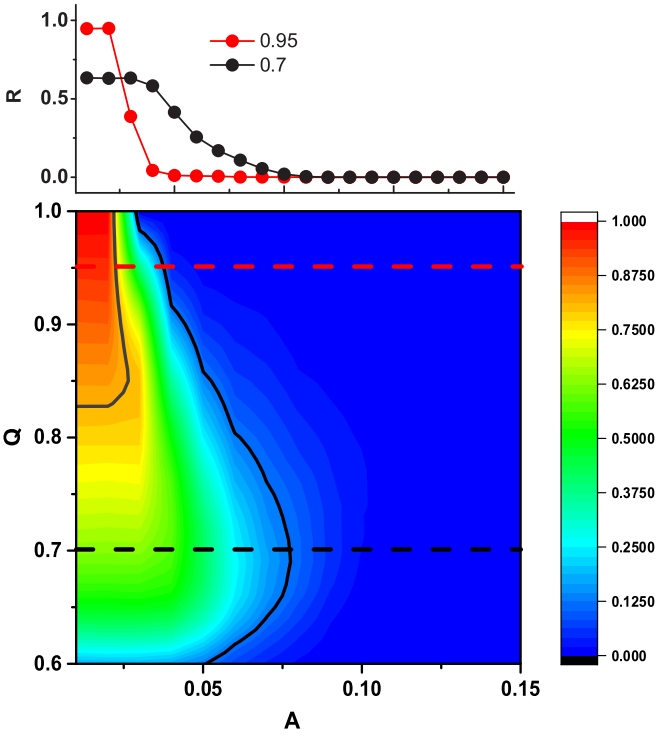

FIG. 9. The phase diagram of SP probability of the tumor number density R with the spatial homogeneity Q and the Allee effect A of a lattice size set to 50×50. In the Q-A parameter space, R can be divided into three phase regions as high, medium, and low penetration regions, respectively. The upper curves are two typical profiles of the phase diagram at $Q = 0.7$ and $Q = 0.95$, respectively.

displacement of the number density of the logistic model and Allee model reveals the growth fronts of both systems move linearly with time and their front speeds are kept constantly. The difference in the two growth-diffusion models in their long-time dynamic behavior is not as salient as that of their short-time counterparts (see Fig. S7 of the SM [19]). However, a full comparison between the short- and long-time dynamic behaviors of both logistic and Allee growth-diffusion systems necessitates some further systematical calculations on more diverse extended percolation lattices, e.g., bond percolation and 3D lattices.

E. Spatiotemporal growth and diffusion features of the Allee model

The Allee model, as we suggested before, is more suitable for describing the growth and infiltration of a early-stage malignant tumor. This section focuses on addressing further the dependence of spatiotemporal growth and diffusion in the Allee model on the spatial homogeneity Q and Allee effect A. Figure 9 exhibits the SP probability R of the tumor number density against the variation of Q and A. According to the trend of R, the parameter space of Q and A can be divided into three regions as the high penetration region (red), the medium penetration region (green), and the low penetration region (blue). Take $Q = 0.95$ and 0.70 as instances for a better explanation. The upper curves in Fig. 9 depict the variation trend of the SP probability R with an increasing Allee effect A at $Q = 0.95$ and 0.70. This graph confirms that the SP probability of the tumor number density will decline to zero with increasing Allee effect. The decline is related to a lack of adaptive cooperation among tumor cells under a strong Allee effect that restrains tumor growth. The region of medium penetration expanding farthest around Q is equal to 0.7, inferring that the transition of a tumor from high penetration to low penetration is a gradual process of a phase transition. In a more homogeneous lattice where Q is greater than 0.9, the range of medium penetration is relatively small, meaning that the transition of a tumor from high penetration to low penetration is a rapid process. When Q approaches 0.6, the medium penetration region shrinks abruptly, causing difficulty in the SP because Q approaches the critical point Q_c. The region of medium penetration reflects the sensitivity of R to parameters Q and A. Note that under a certain degree of spatial homogeneity, e.g., $Q = 0.7$, the medium penetration owns the largest region, and the SP probability R becomes less sensitive to the Allee effect A. The results above indicate that a certain degree of spatial inhomogeneity expedites the diffusion and invasion of a tumor, which can be found in some clinical instances [38,39].

Further analysis reveals what a different influence the Allee effect can exert on short-time growth and diffusion in the GDS. The statistics of the growth and diffusion at $Q = 0.9$ show that the diffusion exponent b increases with the Allee effect, as shown in Fig. 10(a), while the tumor number density declines with the Allee effect instead, as shown in Fig. 10(b). This consequence can be interpreted as the lack of cooperation between tumor cells intensifies

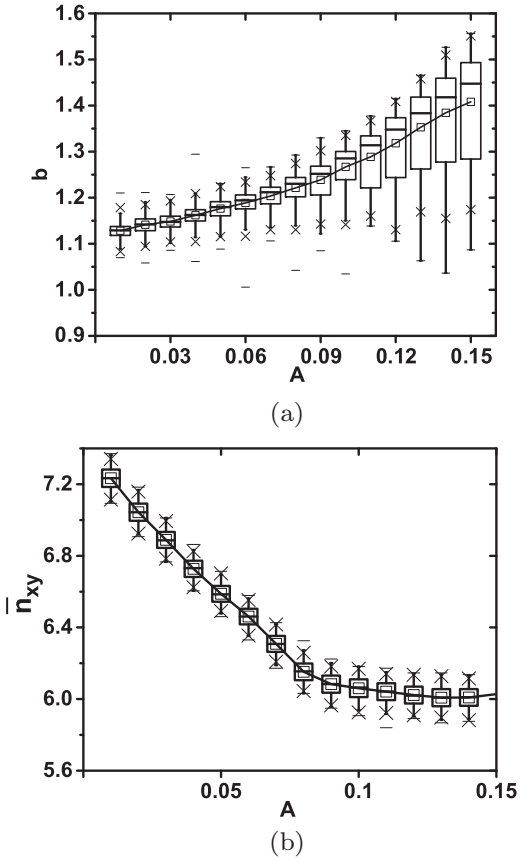

FIG. 10. (a) The diffusion exponent of tumor cells b and (b) the site-averaged tumor number density $\bar{n}_{xy}$ vs the Allee effect A, when the site occupation fraction of a percolation lattice $Q = 0.9$, and the lattice size is set to 50×50.

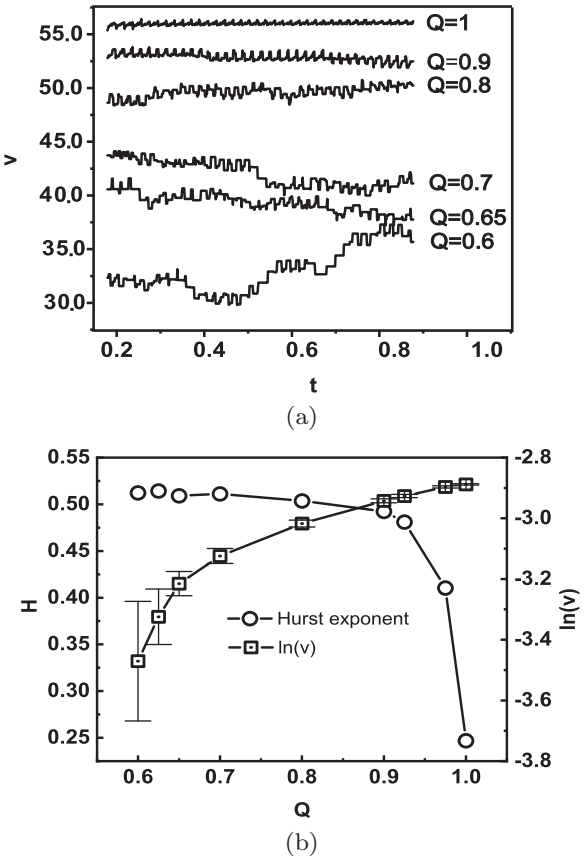

FIG. 11. (a) The average propagation front speed (APFS) for different Q values and (b) the standard deviation the logarithmic APFS.

with the Allee effect, and tumor cells that can successfully penetrate a percolation lattice will decrease in number density even though those cells themselves can diffuse easily. The result above implies that it is less possible for a tumor to diffuse and grow considerably at the same time when the Allee effect becomes strong enough. It is a sort of dynamic diversity that the Allee model introduces to its growth and diffusion in a percolation lattice, and in this situation, a tumor with a better mobility inclines to spread and metastasize rather than proliferate, which has been reported [40] as well as observed in our clinical MRI report (see Figs. S8 and S9 of the SM [19]).The explanation proposed for this is the influence of a variable microenvironment a tumor locates on its growth-diffusion mode, which changes from a proliferative but less diffusible mode to a diffusible but less proliferative mode, which is similar to the adaptive phenotypic transition [41,42]. Besides nasopharyngeal carcinoma (see Figs. S8 and S9 of the SM [19]), a recent study reported that cancer cells such as melanoma cells are usually in a metastasizing state under the effect of a tumor microenvironment [43]. The factors related to the tumor's microenvironment include a low oxygen supply, an inflammatory state, and severe a lack of nutrition. All of them contribute to the Allee effect and significantly impact the adaptive cooperation of spreading tumor cells.

F. Propagation front speed (PFS) of Allee growth

In addition to the root-mean-square displacement of the tumor number density r_n described in Sec. III D, the speed of the propagation front was taken into account in reference to Refs. [44,45]. Specifically, the propagation front of the Allee growth on a percolation lattice was investigated, and the average propagation front speed (APFS), denoted as v, was introduced to characterize the dynamics of the propagation front (see Sec. S11 of the SM [19]).

Figure 11(a) displays the APFS for different Q values. Evidently, the APFS hardly changes over time on a homogeneous lattice ($Q = 1$), but it decreases and fluctuates more drastically with increasing inhomogeneity of the percolation lattice, i.e., declining from $Q = 1$. Bru *et al.* obtained similar results by applying the scaling analysis *in vitro* brain tumors [46], and extensive simulations using realistic parameter values also indicated these results in the research of Menchon and Condat [47]. The Hurst exponent H (see Sec. S11 of the SM [19]) of the APFS as a time series was estimated. The logarithmic APFS $\ln(v)$ was computed. Both H and $\ln(v)$ are averaged results over different initial lattice configurations with the same Q value.

It is shown in Fig. 11(b) that H rises significantly as Q decreases from 1. H equals 0.25 when Q approaches 1, signifying that v oscillates frequently around its mean. Instead, H is above 0.5 when Q declines from 1, indicating that the APFS

oscillates around the mean far less frequently (see Sec. S11 of the SM [19]). It also shows the standard deviation of $\ln(v)$. The analysis of both the Hurst exponent and the logarithmic APFS shows that with respect to the timescale of τ_{ref} (Table I), the propagating front tends to move with a remarkably varying and positively autocorrelative APFS as Q declines from 1.

IV. CONCLUSIONS

This paper addresses the evolution of the spatiotemporal patterns of two different growth-diffusion systems (GDSs), logistic and Allee growth, in a 2D site percolation lattice. The following conclusions are drawn:

(1) Concerning the two GDSs, critical points ($Q_c = 0.59$–0.60) are observed that existed for their penetration probability of the number density R through the percolation lattice, but the Allee effect undermines the critical point in Allee growth. Moreover, the Allee effect reduces the critical exponent value γ but scarcely affects ν. Decreasing γ brings about a decline in the penetration probability R, leading to a significant fluctuation and extreme sensitivity of R at the critical point.

(2) The analysis of the spatiotemporal patterns of the two GDSs, assisted with a clinical image analysis of a breast tumor, suggests that the Allee model is more suitable than the logistic model to describe the malignant growth of an early-stage tumor. The spatial homogeneity Q in combination with the Allee effect A significantly influences the growth and diffusion of the Allee model, as manifested by its distinctive spatiotemporal pattern. The growth and diffusion in the logistic model take on a continuous mode while those in the Allee model present a discrete mode owing to the fluctuation caused by local variable cooperation among the tumor cells. Furthermore, the Allee effect also induces a dynamic diversity in the short-time growth and diffusion in the GDS, resulting in a peculiar trend of opposite curves of growth versus diffusion with an increasing Allee effect. The propagation front of the Allee growth moves on a percolation lattice at a remarkably varying APFS, and the APFS fluctuates less and less frequently as the inhomogeneity of the percolation lattice increases.

(3) The findings in this paper may provide some physical implications for understanding the underlying mechanism of heterogeneous growth, diffusion, and infiltration of an early-stage tumor in medicine.

ACKNOWLEDGMENT

We acknowledge support from the Special Program for Applied Research on Super Computation of the NSFC-Guangdong Joint Fund (the second phase) under Grant No. U1501501, and Tianhe-2 Supercomputing Application Cultivation Projects (Grant No. 74130-18823701) sponsored by National Super Computer Center in Guangzhou.

[1] W. Li, K. Wang, and H. Su, Appl. Math. Comput. **218**, 157 (2011).
[2] M. Costa and L. dos Anjos, Neotrop. Entomol. **44**, 385 (2015).
[3] A. J. Perumpanani, J. A. Sherratt, J. Norbury, and H. M. Byrne, Physica D **126**, 145 (1999).
[4] W.-R. Zhong, Y.-Z. Shao, and Z.-H. He, Phys. Rev. E **73**, 060902(R) (2006).
[5] W.-R. Zhong, Y.-Z. Shao, and Z.-H. He, Phys. Rev. E **74**, 011916 (2006).
[6] M. Greaves and C. C. Maley, Nature (London) **481**, 306 (2012).
[7] K. Böttger, H. Hatzikirou, A. Voss-Böhme, E. A. Cavalcanti-Adam, M. A. Herrero, and A. Deutsch, PLoS Comput. Biol. **11**, e1004366 (2015).
[8] K. S. Korolev, J. B. Xavier, and J. Gore, Nat. Rev. Cancer **14**, 371 (2014).
[9] L. Sewalt, K. Harley, P. van Heijster, and S. Balasuriya, J. Theor. Biol. **394**, 77 (2016).
[10] A. Tsoularis and J. Wallace, Math. Biosci. **179**, 21 (2002).
[11] P. A. Stephens, W. J. Sutherland, and R. P. Freckleton, Oikos **87**, 185 (1999).
[12] S. Kirkpatrick, Rev. Mod. Phys. **45**, 574 (1973).
[13] S. Prager, J. Chem. Phys. **33**, 122 (1960).
[14] D. Stauffer and A. Aharony, *Introduction to Percolation Theory* (Taylor & Francis, London, 1992).
[15] I. M. Sokolov, Soft Matter **8**, 9043 (2012).
[16] M. H. A. S. Costa, A. D. Araújo, H. F. da Silva, and J. S. Andrade, Jr., Phys. Rev. E **67**, 061406 (2003).
[17] M. T. Gastner, B. Oborny, A. B. Ryabov, and B. Blasius, Phys. Rev. Lett. **106**, 128103 (2011).
[18] D. A. Hormuth, J. A. Weis, S. L. Barnes, M. I. Miga, E. C. Rericha, V. Quaranta, and T. E. Yankeelov, J. R. Soc. Interface **14**, 20161010 (2017).
[19] See Supplemental Material at http://link.aps.org/supplemental/10.1103/PhysRevE.99.042401 for details on the numerical methods and clinical MRI diagrams.
[20] R. Law, D. J. Murrell, and U. Dieckmann, Ecology **84**, 252 (2003).
[21] C. M. Taylor and A. Hastings, Ecol. Lett. **8**, 895 (2005).
[22] P. J. Pal, T. Saha, M. Sen, and M. Banerjee, Nonlinear Dyn. **68**, 23 (2012).
[23] K. Kato, S. Todo, K. Harada, N. Kawashima, S. Miyashita, and H. Takayama, Phys. Rev. Lett. **84**, 4204 (2000).
[24] J. D. Murray, Biomathematics **19**, 261 (2002).
[25] S. C. Wei, L. Fattet, J. H. Tsai, Y. Guo, V. H. Pai, H. E. Majeski, A. C. Chen, R. L. Sah, S. S. Taylor, A. J. Engler *et al.*, Nat. Cell Biol. **17**, 678 (2015).
[26] G. Sciumè, R. Santagiuliana, M. Ferrari, P. Decuzzi, and B. Schrefler, Phys. Biol. **11**, 065004 (2014).
[27] A. R. Anderson, Math. Med. Biol. **22**, 163 (2005).
[28] A. R. Anderson, M. A. Chaplain, E. L. Newman, R. J. Steele, and A. M. Thompson, Comput. Math. Methods Med. **2**, 129 (2000).
[29] Y. Kim, S. Lawler, M. O. Nowicki, E. A. Chiocca, and A. Friedman, J. Theor. Biol. **260**, 359 (2009).
[30] R. A. Gatenby and E. T. Gawlinski, Cancer Res. **56**, 5745 (1996).
[31] K. Binder, Ferroelectrics **73**, 43 (2011).

[32] J. Hauke and T. Kossowski, Quaestiones Geographicae **30**, 87 (2011).
[33] R. Haining, Geogr. Anal. **23**, 210 (2010).
[34] Z. Yong, Y. Zi-Qing, Z. Xin, and C. Xiao-Song, Commun. Theor. Phys. **64**, 231 (2015).
[35] T. Tél, Á. Fülöp, and T. Vicsek, Physica A **159**, 155 (1989).
[36] R. Lopes and N. Betrouni, Med. Image Anal. **13**, 634 (2009).
[37] R. Metzler and J. Klafter, Phys. Rep. **339**, 1 (2000).
[38] T. Yu, K. Liu, Y. Wu, J. Fan, J. Chen, C. Li, G. Zhu, Z. Wang, and L. Li, Int. J. Mol. Med. **32**, 1093 (2013).
[39] N. F. Boyd, G. A. Lockwood, J. W. Byng, D. L. Tritchler, and M. J. Yaffe, Cancer Epidemiol. Biomarkers Prev. **7**, 1133 (1998).
[40] A. Farin, S. O. Suzuki, M. Weiker, J. E. Goldman, J. N. Bruce, and P. Canoll, Glia **53**, 799 (2006).
[41] C. A. Klein, Nature (London) **501**, 365 (2013).
[42] A. Hoshino, B. Costa-Silva, T. L. Shen, G. Rodrigues, A. Hashimoto, M. M. Tesic, H. Molina, S. Kohsaka, G. A. Di, and S. Ceder, Nature (London) **527**, 329 (2015).
[43] P. Falletta, L. Sanchez-del Campo, J. Chauhan, M. Effern, A. Kenyon, C. J. Kershaw, R. Siddaway, R. Lisle, R. Freter, M. J. Daniels *et al.*, Genes Dev. **31**, 18 (2017).
[44] K. R. Swanson, E. C. Alvord, and J. D. Murray, Cell Prolif. **33**, 317 (2000).
[45] L. Hathout, B. M. Ellingson, T. Cloughesy, and W. B. Pope, Int. J. Oncol. **46**, 825 (2015).
[46] A. Brú, J. M. Pastor, I. Fernaud, I. Brú, S. Melle, and C. Berenguer, Phys. Rev. Lett. **81**, 4008 (1998).
[47] S. A. Menchón and C. A. Condat, Phys. Rev. E **78**, 022901 (2008).